

A Wavefront Tilt Correction Servo for the Sydney University Stellar Interferometer

Theo A. ten Brummelaar* and William J. Tango
Chatterton Astronomy Department, School of Physics
University of Sydney

Experimental Astronomy, Vol 4, 297-315 (1994)

Abstract

The tilt correction servo for the Sydney University Stellar Interferometer (SUSI) consists of a 'pyramid' detector and piezo-electrically controlled tilt mirrors. The system measures image position and re-centers it with a sample frequency of 1000 Hz thereby holding the two beams of the interferometer parallel with a standard deviation of 0.164 ± 0.025 arcseconds. With an aperture size of 0.06 metres this implies less than a 2% loss in the visibility measurements made by SUSI. The servo has been used to magnitude 6.5 stars and is predicted to have a limiting magnitude of 7.5 and possibly as high as 8.5. The system not only corrects for the tilt introduced by the atmosphere but will supply a good estimate of seeing conditions using the same optical path through the atmosphere as the visibility measurements of the interferometer.

1 Introduction

The recently constructed Sydney University Stellar Interferometer (SUSI)[6, 5, 7] at Narrabri, N.S.W. in Australia is an optical Michelson stellar interferometer which operates in the range 400-800 nm and can be used with baselines ranging from 5 m to 640 m. In order to detect fringes with a Michelson type interferometer it is important to keep the wavefront distortion caused by atmospheric turbulence to a minimum. In SUSI this is done by restricting the aperture to r_0 or less, thereby sampling a basically flat but tilted wavefront; the residual tilts are then removed by a tilt correcting servo which is the subject of this paper.

The maximum useable aperture for the interferometer is 140mm; smaller aperture sizes can be selected depending on the average value of r_0 during the night. As SUSI currently operates in the blue region of the spectrum r_0 is typically less than 100mm. Any residual wavefront tilts will cause a reduction in the measured fringe visibility, and the basic function of the digital tilt correction servo is to remove these tilts in the two incoming light beams, thereby keeping the interfering beams from the two arms parallel. The r.m.s. visibility

*Now with the Center for High Angular Resolution Astronomy, Georgia State University.

resulting from losses caused by small tilt errors when the beams are combined is given by Buscher [3] as

$$\eta = 1 - 1.8\langle(\theta/\theta_0)^2\rangle \quad (1)$$

where θ is the total differential tilt error and θ_0 is the angular radius of the Airy disc formed by the stellar image ($1.22\lambda/D$). Thus in order to ensure these losses are less than 5% the tilt servo must keep the two beams to within 0.167 the size of the Airy disc radius. Assuming the positions of the two beams at any given time are independent variables with a normal distribution (see section 4), each beam needs to be stable to within 0.118 of the size of the Airy disc. For example, to keep visibility losses due to tilt less than 5% for an aperture diameter of 60mm, the tilt servo must keep the beams parallel to within 0.31 arcseconds, which requires a single beam stability of 0.22 arcseconds. As will be shown in section 3 the tilt servo exceeds this criterion.

The servo must track a star image to this precision with a bandwidth large enough to include most of the spectrum of the tilt fluctuations caused by the atmosphere. The servo should not be sensitive to frequencies higher than this as the only tilt changes it will be responding to are those caused by photon noise. Choosing a servo bandwidth is thus a compromise between complete coverage of the tilt spectrum and the amplification of photon noise. The range of frequencies required is of the order of tens of hertz extending as far as perhaps 50 hertz [11, 15]. The sample time of the tilt servo must therefore be quite small, at least 10ms or less, although longer sample times will be possible during times of relatively good seeing. The requirement of high speed has implications for the detectors used, the electronics and the computational hardware and algorithms.

A further requirement of the tilt servo is that its limiting magnitude should be as large as possible. If the tilt servo fails, the entire interferometer will fail; the tilt servo defines the limiting magnitude of SUSI. The tilt correction system must also operate in the optical waveband of the rest of the instrument. Both these criteria have implications for the glass, coatings, detection system and electronics.

The final requirement of the tilt servo is that it should be capable of logging data for analysis of seeing conditions and atmospheric turbulence. This is done by the computer control system. This information is used, for example, to estimate r_0 and to select the appropriate working aperture for the interferometer. Some results obtained by the tilt system while tracking stellar sources and methods for data reduction are presented in section 4.

2 Description of Hardware

While it is not the intent of this paper to describe the entire optical system of SUSI a brief description follows in order that the positioning of the wavefront tilt servo components can be described. Figure 1 contains a sketch of the optical layout of SUSI. After being guided into the vacuum system by the siderostats and passing through the beam reducing telescope (BRT) the star light is corrected for atmospheric dispersion (ARC) and then either enters the optical path length compensator (OPLC) or is diverted towards the star acquisition camera. The tilt/tilt mirrors are at either end of the OPLC enclosure. Since the path length compensation is performed in air the longitudinal dispersion corrector (LDC) is added to the optical chain after the OPLC. The light is then directed onto the optical table where

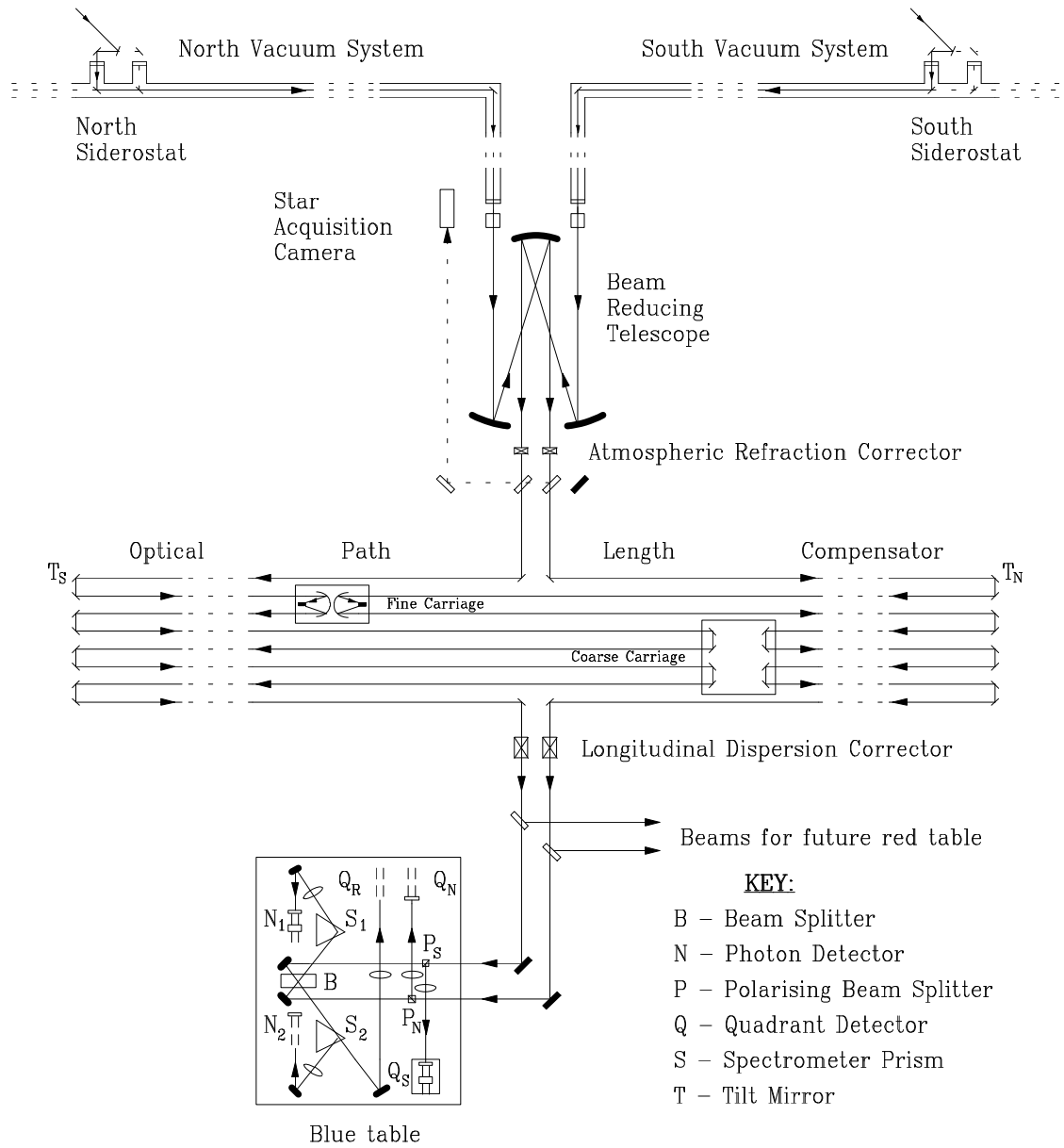


Figure 1: A diagram (not to scale) of all the major optical components of SUSI.

polarising beamsplitters divert half the light to the quadrant detectors of the tilt servo and the other half towards the main beamsplitter. Note that one of these interference beams can be diverted to the reference quadrant detector for interferometer alignment.

The key elements of the optical system of the wavefront tilt servo are the “optical pyramids”, located on the optical table and used to detect the tilt errors, and the tip/tilt mirrors, located at either end of the OPLC, which correct the residual tilts. These are described in the following sections.

In order to meet the requirement specification set out in section 1 both the detectors and mirrors must have resolutions of a fraction of an arcsecond. Furthermore, to track an analogue phenomenon such as image position with a digital system the cycle time of detection, calculation and correction must be less than the time constant of the tilt fluctuations. There is unfortunately no agreed definition for the characteristic time scale t_0 for atmospheric phase fluctuations, but the data of Roddier et al [12] and Nightingale & Buscher [10] suggest that it is of the order of a few milliseconds. Consequently, a basic 1 millisecond sample time was chosen for the control computer. Sample times which are multiples of this minimum are also available.

2.1 The Optical Pyramids

The optical pyramids split the image of the star into four parts by focusing the stellar image onto two separate knife edges, one vertical and one horizontal. Each knife edge is created by a prism made from two optically contacted rhombs constructed from BK-7 glass. Light is first focused onto the vertical edge and the split images are refocused onto the horizontal edge by two small lenses. Field lenses finally image the pupils onto four photomultiplier tubes. The detected photon events from each tube are summed into registers and the number of counts measured during each basic sample time is transferred to the control computer for processing by the servo software. After application of a gain correction, any imbalance in the four quadrant signals indicates a tilt error. The actual signals correspond to the vertical and horizontal components of the tilt error. Since all surfaces have coatings optimised in the blue, throughput should be greater than 90%. Simultaneous photometric measurements using the quadrant detectors and the visibility measurement system confirmed this. The prisms, lenses and mounts were originally designed by one of us (WJT) for an 11.4m prototype interferometer [4].¹ Refer to Fig. 2 for a drawing of the detector optics.

The entire optical pyramid is mounted on an x/y or vertical/horizontal platform which can be remotely motor driven. The motor drives have been installed on the two detectors used in the tilt servos for the north and south beams while a third ‘reference’ detector is in principle fixed and defines the optical axis of SUSI. The tilt correcting servo detectors are optically superimposed with this reference detector and the beams emerging from the main beam combiner are accurately parallel.

In order to test the detector response, an optical configuration using an autocollimated laser was used. With neutral density filters in place to reduce the light intensity so that the photomultipliers could be switched on, the image position as measured by the quadrant

¹The design was based on a similar system used by R. Q. Twiss for an interferometer originally built at the National Physical Laboratory (UK) and later rebuilt at the Italian outstation of the Royal Observatory Edinburgh [13].

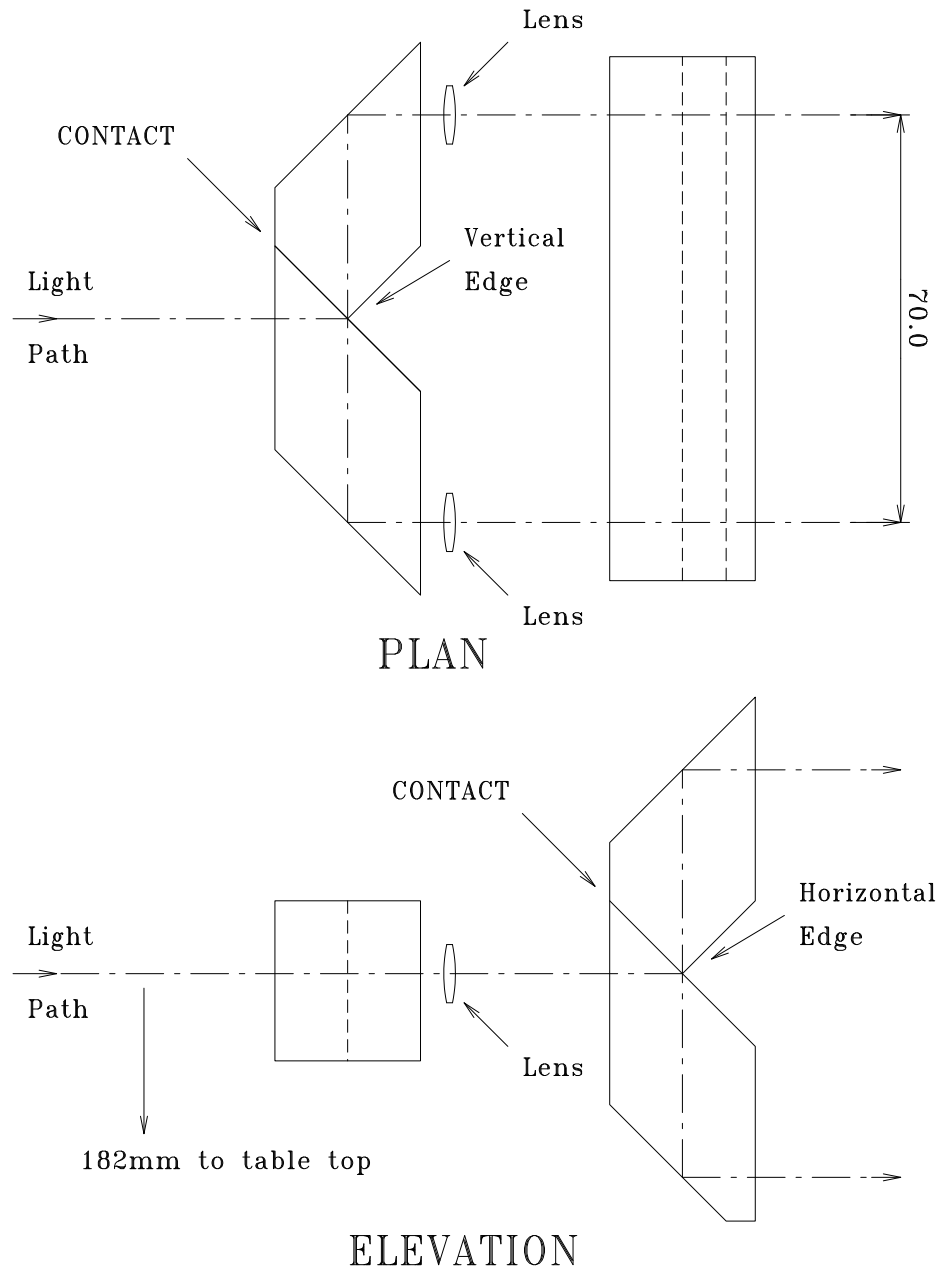


Figure 2: Plan and elevation of quadrant detector optics used in SUSI. The dashed line represents the light path through the optical system. Dimensions in mm.

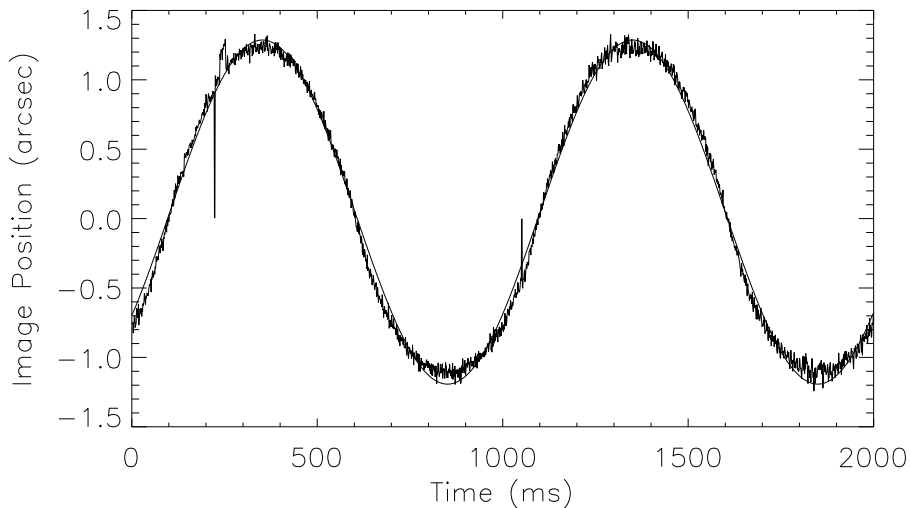


Figure 3: Measured response of one axis of a quadrant detector given a 1Hz sine wave input. The smooth line is a least squares fit of a sine wave to the data. It is clear the response of the detector is very close to linear for deviations small compared to an Airy spot, as predicted. The noise represents an angular variation of less than 0.1 arcseconds. The large spikes in the plot above were due to software timing errors which have since been corrected.

detectors was monitored while a sine wave was used to drive the tilt mirrors. The frequency of the sine wave was 1 Hz and the amplitude was set so the signal stayed well within the range of the detectors. A sample of the results is shown in Fig. 3 along with a least squares fit of the data. The RMS residual after fitting was 0.1 arcseconds. This same experiment was performed on all detectors and axes with similar results.

The error associated with angular position measurements using quadrant detectors, as well as for other optical detectors used for adaptive optics, has been well studied [8, 14, 16]. The expression for the error term associated with the quadrant detector is

$$\sigma_{\phi} = \pi \left[\left(\frac{3}{16} \right)^2 + \left(\frac{n}{8} \right)^2 \right]^{\frac{1}{2}} \frac{\left(\frac{\lambda}{D} \right)}{\text{SNR}} \quad (2)$$

where n is the angular subtense of the object divided by the diffraction angle (λ/D) of the optical system, D is the aperture diameter and SNR is the signal to noise ratio of the four detectors summed to act as a single detector. In the system under discussion here the star is unresolved and we therefore say $n \ll 1$. The signal to noise ratio of the four detectors summed is primarily dependent upon the Poisson statistics of the photon events so we can write the error in angular position measurement of the quadrant detectors as

$$\sigma_{\phi} = \frac{\pi \frac{3}{16} \left(\frac{\lambda}{D} \right)}{\sqrt{N}} \quad (3)$$

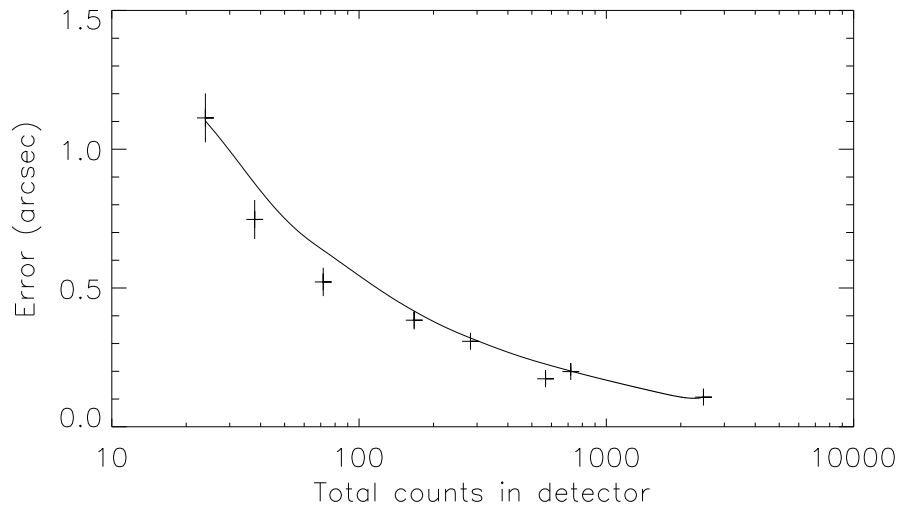


Figure 4: The solid line in the plot above represents the theoretical standard deviation of detected position in a quadrant detector as stated in Eq. (3). The points plotted are measured values with the error bars representing the uncertainty in detector calibration. The points plotted cover a range of aperture sizes from 1 to 2.5 cm using the laser wavelength of 442nm. Correspondence is good, giving us confidence in the analytical expression.

where N is the total number of counts received in all four quadrants. In order to test this relationship several two second samples were taken of detector response for a range of light intensities. The resulting data were Fourier transformed, the low spatial frequencies attenuated, and inverse transformed back to the spatial domain. These operations were performed in order to filter out any underlying motion of the beam due to internal thermal and turbulent effects. Once filtered, the variance of each sample was calculated and compared to a prediction using Eq. (3) (See Fig. 4). This plot demonstrates that Eq. (3) can be used to estimate the error in angular position detection of the quadrant detectors. It was discovered that the throughput of the prisms was different when the spot was fully within any given quadrant than when it was evenly divided between them. This was attributed to the fact that the ‘knife edges’ have a finite extent and may have irregularities. Other than this, edge imperfections do not seem to affect the signal to noise performance of the device. This could be attributed to the fact that the image scale on the knife edges is of the order of 0.1mm which is large compared to any edge thickness or imperfections.

2.2 The Tip/Tilt Mirrors

To correct wavefront tilt in an incoming collimated beam adaptive mirrors are required which can be set to any angular position under computer control. As with the pyramids, the mirrors were originally made for the prototype stellar interferometer. The adaptive mirror system consists of a 70 mm diameter flat mirror mounted on three piezo-electric transducers (PZTs)

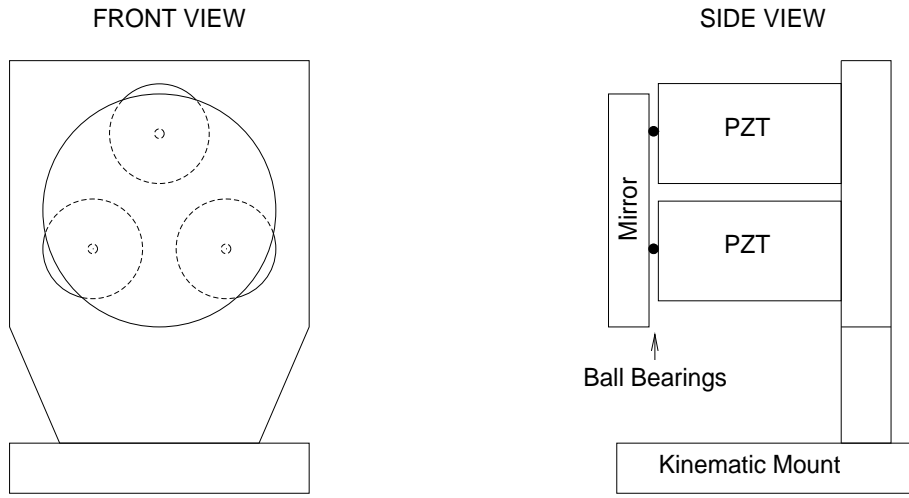


Figure 5: Design sketch of the tip/tilt mirrors used in SUSI.

arranged at the vertices of an equilateral triangle. By sending the appropriate signals to these actuators the mirror can be tilted in any direction while minimising any piston motion. A plate with three vertical adjustable screws holds the entire mirror assembly so the central mirror position can be correctly aligned with the rest of the optical system. Small ball bearings are glued to the end of the actuators which in turn are glued to the back of the mirror. A design sketch of the mirrors is given in Fig. 5.

A simple circuit converts the horizontal and vertical tilt errors into the appropriate actuating signals which are applied to the PZT high voltage amplifiers. The amplifiers have a bandwidth greater than 100 Hz for actuating signals with rms values corresponding to a few arcseconds of tilt (because of large capacitance of the load the large signal amplifier response has a smaller bandwidth).

This adaptive optics system is a zero seeking servo and therefore the absolute calibration factors need not accurately be known. However, to use mirror positions to study atmospheric turbulence the mirrors need to be calibrated. Using the mirrors to calibrate the detectors will also help in selecting appropriate servo parameters.

Since the angles involved are so small it was decided to use the interferometer itself for these measurements by sampling tilt fringes. Not only is this method very precise but it also means the mirrors are calibrated *in situ* using exactly the same electronics and optics as will be used during an astronomical observation. The relationship between the spatial frequency of the tilt fringes ω_0 and the mirror position θ_{mirror} is

$$\theta_{\text{mirror}} = \frac{\lambda\omega_0}{4} \quad (4)$$

where λ is the laser wavelength (442nm). The resulting fringe pattern sampled by a CCD and frame grabber was modelled using the equation [1]

$$I = I_1 + I_2 \cos^2(\pi\omega_0(x \cos \phi + y \sin \phi) + \delta). \quad (5)$$

The angle ϕ represents the orientation of the fringes, the intensities I_1 and I_2 are for the background light and fringe amplitude respectively and the δ term incorporates any fringe phase offset. Sampled data was fitted to Eq. (5) in the least squares sense. An example of sampled tilt fringes and the resulting fit can be found in Fig. 6.

The results for one mirror axis are shown in Fig. 7. This experiment confirmed that the positioning of the mirrors was linear. Based on this set of calibration data it is possible to measure image position on the sky to within ± 0.1 arcseconds.

This calibration procedure does not provide information about the dynamic response of the mirror. Further, it is difficult to estimate from the fringes whether there is any significant ‘‘piston’’ component in the mirror motion (an overall linear displacement of the mirror is referred to as piston motion and it is undesirable in an interferometer, since it introduces additional phase noise). A commercial metrology laser system (Hewlett-Packard model 5501A) was used to measure the movement of the mirror centers while they were being driven. The piston movement was found to be less than approximately 2 nm per arcsecond of mirror tilt. The dynamic response of the mirror system is discussed in section 3.3.

3 System Model and Performance

Since the tilt correction system can be described as a zero seeking servo, its behavior is subject to linear control theory. A diagram of the tilt correction servo viewed as a negative feedback system is given in Fig. 8. The error signal $E(s)$ represents the resulting angle between the beam and the optical axis of the interferometer. This is measured by the quadrant detectors, whose transfer function is $D(s)$, and processed by the control computer with the transfer function $F(s)$. The gain component of the feedback loop is therefore

$$G(s) = D(s)F(s). \quad (6)$$

The output of the control computer, $o(t)$ is a number between -1 and $+1$ and represents a normalised measurement of the tilt of the incoming beam. If this number is multiplied by the mirror calibration constant K_m the results can be recorded in the correct units and stored for later processing and analysis.

The normalised beam tilt measurement is processed by the high voltage amplifier $A(s)$ and subtracted from the optical beam by the tilt mirror $M(s)$. The feedback component of the system is therefore

$$H(s) = A(s)M(s). \quad (7)$$

There are two transfer functions of primary interest. The first transfer function describes the ability of the mirror $B(s)$ to track the real tilt of the beam $R(s)$ defined

$$T_{\text{track}}(s) \equiv \frac{B(s)}{R(s)}. \quad (8)$$

We shall use this transfer function to study how well the system actually removes tilt. The second transfer function of interest is

$$T_{\text{measure}}(s) \equiv \frac{C(s)}{R(s)} \quad (9)$$

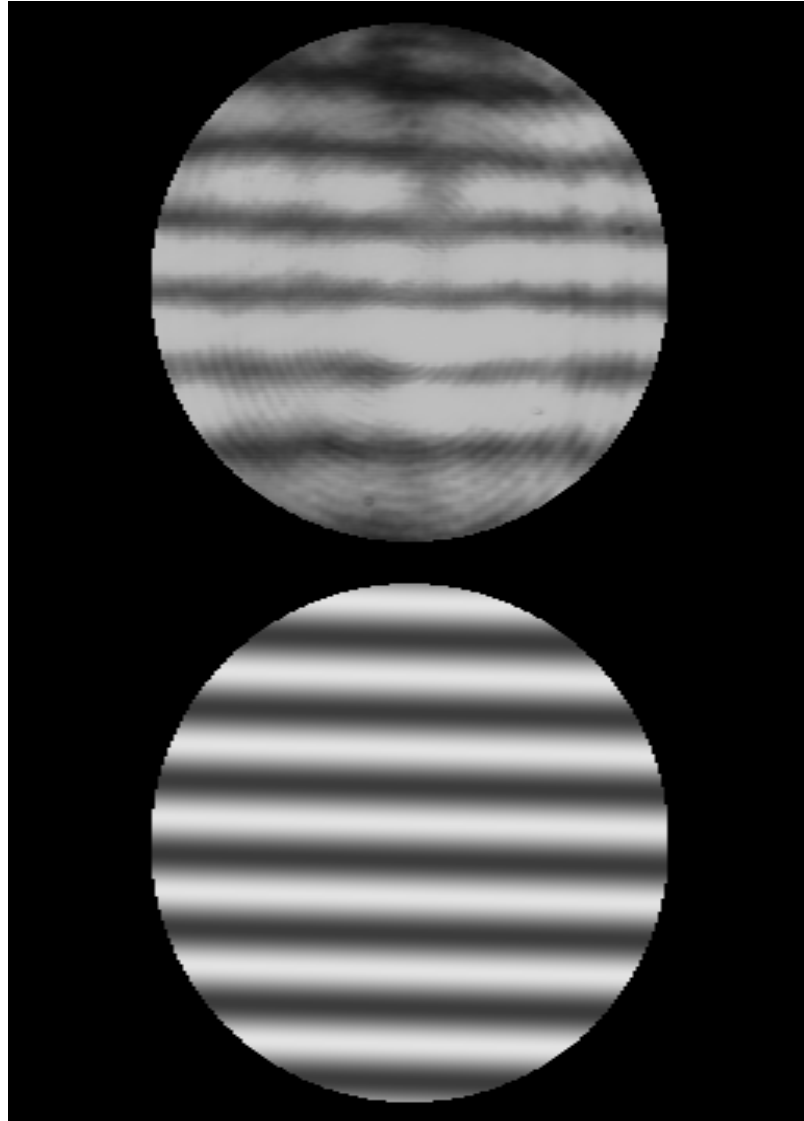


Figure 6: An example set of sampled tilt fringes (top) and the resulting fit (bottom). The circular ring pattern in the sampled data is the result of diffraction and is not modelled. The spatial frequency of these fringes is a measure of mirror tilt and can be read straight out of the fitted data.

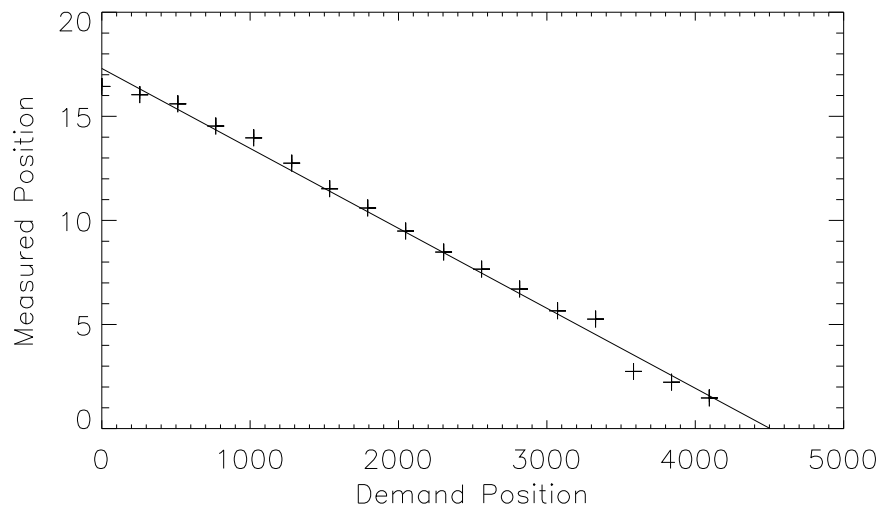


Figure 7: The response of one axis of one of the tilt mirrors The vertical axis is in arcseconds, the horizontal axis is in arbitrary DAC units and the vertical lines are error bars. A fit to this plot results in a calibration constant of $K_m = -3.84 \pm 0.08$ milliarcseconds per DAC unit.

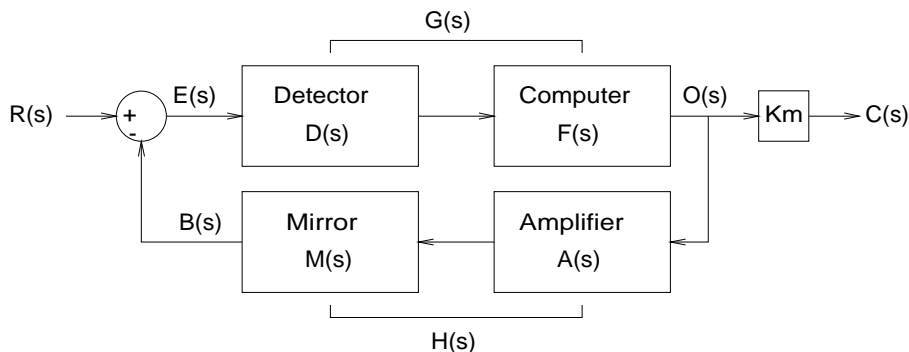


Figure 8: The tilt correction servo analysed as a negative feedback loop. The tilt of the incoming beam is $R(s)$, the corrected output beam going on to the rest of the optical table is $E(s)$ while the output of the computer system, which represents a measurement of wavefront tilt, is $C(s)$. The ‘subtraction’ is performed by the tilt mirror itself. The final multiplication of the computer output by the mirror calibration constant K_m , ensures that the output of the system is in the same units as the input.

which describes the ability of the system to measure the incoming beam tilt. Using standard servo analysis it can be shown that these transfer functions are

$$T_{\text{track}}(s) = \frac{G(s)H(s)}{1 + G(s)H(s)} \quad (10)$$

and

$$T_{\text{measure}}(s) = \frac{K_m G(s)}{1 + G(s)H(s)}. \quad (11)$$

Equations (10) and (11) will enable the determination of the usable servo bandwidth for tracking and measurement of beam tilt.

The transfer function of the control computer can be directly calculated, while those of the high voltage amplifier, detectors and mirrors need to be modelled and fitted to experimental data. Once these empirical parameters and transfer functions are known the complex gain of the adaptive optics system can be found and its performance analysed.

3.1 Detector Model

The quadrant detectors measure the beam tilt $\theta_{v,h}(t)$, with the Laplace transform $E_{v,h}(s)$, and produce a normalised output variable $\phi_{v,h}(t)$, with the Laplace transform $\Phi_{v,h}(s)$. As the vertical and horizontal systems are identical, we will drop the v and h subscripts. The equation representing the response of the detector is $\theta(t) = K_d\phi(t)$, so the transfer function of the detector system can be written as

$$D(s) \equiv \frac{\Phi(s)}{E(s)} = \frac{1}{K_d}. \quad (12)$$

Where K_d is the calibration constant for the detector. This expression is correct only if the angular error of the beam is small. If this is not the case the detectors become extremely non-linear and will no longer be stationary, making linear analysis impossible. During normal operation of the servo errors of this kind should not occur.

3.2 Computer System Model

The sole component of the system that can easily be adjusted is the software running in the control computer. Since this software is by definition not an analogue phenomenon Laplace transforms can not be used to analyse its behavior. Instead we shall use the equivalent for sampled data known as the \mathcal{Z} transform [9]. The programme receives a modulated and sampled signal ϕ_k as input representing the normalised beam tilt $\phi(t)$ averaged over the last millisecond which can be approximated by

$$\phi_k = \phi(t)\delta(t - kT) \quad (13)$$

where T is the sample time of 1 ms. This series of samples, which we assume to have the \mathcal{Z} transform $\Phi(z)$, must be processed in some manner by the computer and sent out as the output signal o_k with the \mathcal{Z} transform $O(z)$. The algorithm used in the control computer,

using C_1 as the constant of proportionality, C_2 as the damping constant and T_d as the time over which a running mean is calculated is

$$\underbrace{O_k - O_{k-1}}_{\text{Change in output}} = \underbrace{\frac{C_1 T}{T_d} \sum_{j=1}^{T_d/T} \phi_{k-j}}_{\text{Proportional term}} - \underbrace{C_2(O_{k-1} - O_{k-2})}_{\text{Damping term}}. \quad (14)$$

This is the digital equivalent of a proportional-differential (PD) controller. It is more common to add an integral term to these algorithms although such a ‘PID’ equation has not been used. The output signal of the computer control system is used by another servo controlling siderostat motion. This second ‘slow tracking’ servo uses an integration of the tip/tilt information as an error signal. Consequently an integral term is not included directly in the tip/tilt servo. The \mathcal{Z} transform of Eq. (14) is

$$O(z) - z^{-1}O(z) = \frac{C_1 T}{T_d} \sum_{j=1}^{T_d/T} z^{-j} E(z) - C_2(z^{-1}O(z) - z^{-2}O(z)) \quad (15)$$

which means the transfer function must be

$$F^*(z) \equiv \frac{O(z)}{E(z)} = \frac{\frac{C_1 T}{T_d} \sum_{j=1}^{T_d/T} z^{-j}}{1 - (C_2 - 1)z^{-1} - C_2 z^{-2}}. \quad (16)$$

where the superscript * has been added to make it clear that this is a \mathcal{Z} transform transfer function. The equivalent analogue form for this expression is found by invoking the modulation model [9] and replacing z by e^{-sT} resulting in

$$F(s) = F^*(e^{-sT}) = \frac{\frac{C_1 T}{T_d} \sum_{j=1}^{T_d/T} e^{-jsT}}{1 - (C_2 - 1)e^{-sT} - C_2 e^{-2sT}}. \quad (17)$$

3.3 High Voltage Amplifier and Tilt Mirror Model

Texts that describe the modelling of piezo controllers, such as Tyson [15], state that a damped harmonic oscillator or simple low pass filter is the most appropriate model. After measuring the mirror response it was found that the high frequency response is greater than is predicted by a simple lag system. In an attempt to model this, a second differential term was added to the equation describing a low pass filter. The resulting form of the differential equation representing the combination of the amplifier and mirror is

$$b(t) = \underbrace{\underbrace{K_m o(t)}_{\text{Proportional}} - \tau_A \frac{db(t)}{dt}}_{\text{LowPassFilter}} + \underbrace{K_m \tau_M \frac{do(t)}{dt}}_{\text{Correction}} \quad (18)$$

with the transfer function

$$H(s) = \frac{K_m(1 + \tau_M s)}{1 + \tau_A s}. \quad (19)$$

One way of interpreting this correction factor is to assume there is a resonance in the mirror system with a frequency greater than a few hundred hertz. The simple linear correction term can be seen as a model of the tail end of this resonant peak. It was not possible to directly measure this resonance as it occurs beyond the bandpass of the high voltage amplifiers. The values of the two time constants τ_M and τ_A are will be determined in the following section.

3.4 Frequency Response Measurements

By combining Eqs. (6), (12), (17) and (19) with either (10) or (11) we can derive the theoretical servo response for tracking or measuring beam tilt. However, there are still three parameters not known to great precision. Two of these are the time constants in the feedback circuit, τ_A and τ_M and the third is the detector calibration constant K_d .

Using a laser and spatial filter as an artificial star and an autocollimation mirror added at the end of the optical system many frequency response measurements were carried out on the tilt servo for a wide range of servo parameters. These tests include the entire internal air path of the interferometer. The internal seeing was measured by monitoring the mirror signals with the servo locked on and was found to be less than 0.1 arcseconds. The lowest value of C_1 was the smallest possible while still allowing the servo to function and the highest C_1 value used was the largest value possible without allowing the system to oscillate. The values for C_2 ranged from 0 (no damping) to 1, the point at which the damping algorithm becomes unstable. These experiments resulted in more than 60 000 data points. Although the air inside the optical enclosure was allowed to settle for a number of hours before the experiment commenced, residual air turbulence remained, causing bad signal to noise ratios in the low frequency parts of the measurements. For this reason non-repeatable peaks in these data were smoothed out. A sample of the raw and fitted data is given in Fig. 9. After fitting the theoretical response expressed in Eq. (11) the final values found were

$$\begin{aligned}
 K_d &= 1.7 \pm 0.3 \text{ arcsec} \\
 \tau_A &= 2.2 \pm 0.2 \times 10^{-3} \text{ s} \\
 \tau_M &= 2.2 \pm 0.2 \times 10^{-4} \text{ s} \\
 \text{RMS residue} &= 0.08 \text{ dB}
 \end{aligned}$$

where the errors quoted are the changes required to double the RMS residue of the fit. Given this model appropriate servo parameters C_1 , C_2 and T_d can be chosen to produce the total counts, and therefore signal to noise ratio, and bandwidth required for the prevailing conditions. Using Eq. (10) and imposing the constraints that the resonant peak of the response be no greater than 3dB and the maximum phase lag be less than 45° a maximum tracking bandwidth of 70Hz was found for the system.

It is interesting to note that the largest measurement bandwidth found possible was 160 Hz, which coincides with the cutoff frequency of the high voltage amplifiers. Assuming there is plenty of light available, the response of the system is restricted by the performance of the tilt mirrors themselves. If the current mirrors were replaced with one of the newer piezo systems available today, superior system performance could be achieved.

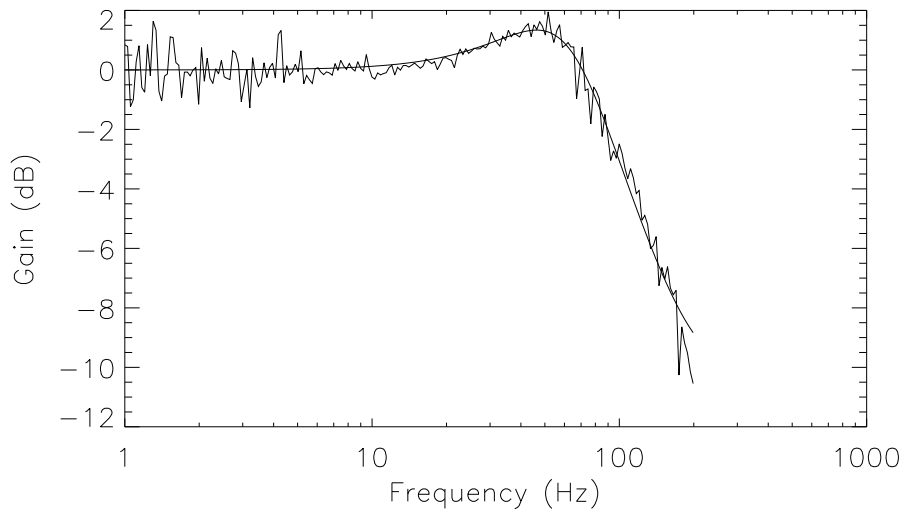


Figure 9: The results of one frequency response measurement of the servo system along with the modelled response for the same parameters.

3.5 Servo Performance

It remained to measure the real performance of the tilt servo to ensure it meets the original specification put forward in section 1. Many trials were used on real star light with stellar magnitudes ranging to magnitude 6.5, sample times ranging from 1 to 30 ms and seeing conditions ranging from 0.8 to over 2 arcseconds. The residual errors measured by the north and south detectors were then summed. A Gaussian curve was then fitted to these data resulting in a standard deviation of 0.098 ± 0.013 arcseconds for the southern system and 0.132 ± 0.010 arcseconds for the northern system. This means that the standard deviation of the difference in tilt between the two beams is 0.164 ± 0.025 arcseconds. By using Eq. (3) it was found that a substantial fraction of this error is due purely to photon noise in the detector. The resulting error in visibility measurement for the apertures currently available on SUSI are listed in table (1). Apart from the largest aperture size currently available of 6cm, all percentage errors in this table are below 5%, showing that the tilt system performs well within the specification set out in section 1. On nights of good seeing and with the largest aperture, the performance of the servo would be expected to be better than the average figure quoted above.

As a final demonstration of the performance of the tilt servo, refer to Fig. 10. Using the same configuration as that used for the servo analysis, a square wave was tracked in auto-collimation on all four axes of the system simultaneously. The results of this demonstration showed good tracking performance with a standard deviation of only 0.02 arcseconds.

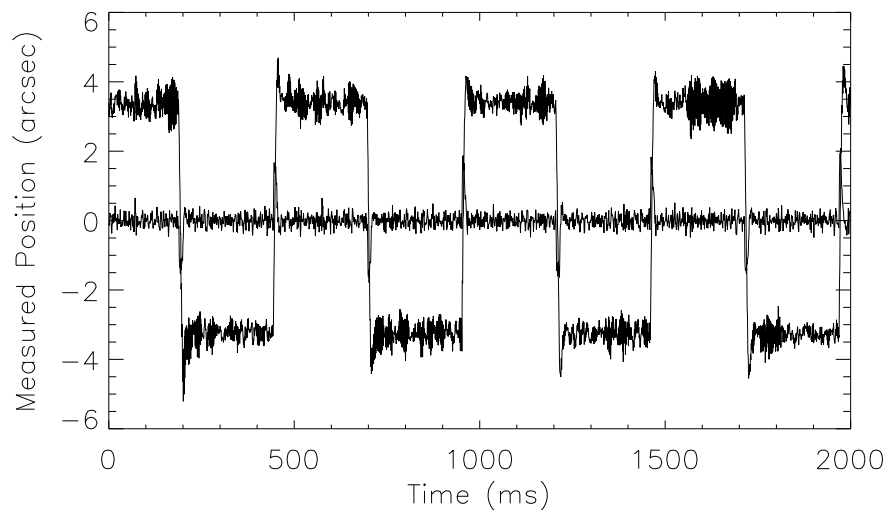


Figure 10: The mirror positions (large movement) and detector positions (small movement) are shown for one axis of a mirror tracking a square wave signal with an amplitude of approximately 3 arcseconds. The residual error as measured by the detectors has an average standard deviation of 0.02 arcseconds across all axes.

Aperture Radius on sky (cm)	Percentage Error of visibility due to residual tilt
0.9	0.1%
1.5	0.4%
2.3	0.8%
3.0	1.4%
3.8	2.3%
6.0 (Maximum)	5.7%

Table 1: The percentage error in visibility measurement caused by residual tilt for the range of aperture sizes currently available on SUSI. (1).

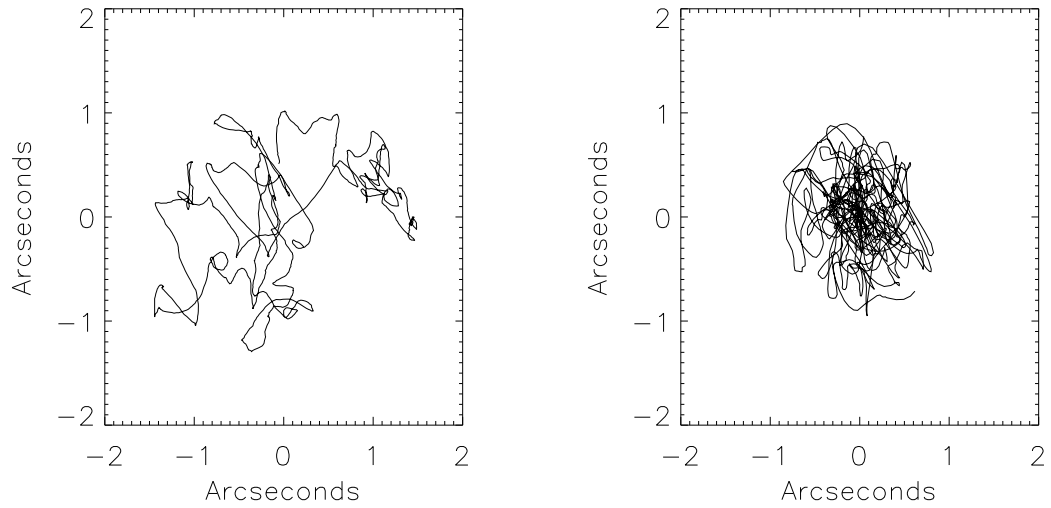


Figure 11: The two plots above show the mirror movement required to track a stellar image for two separate 2 second samples. The left plot is an example of ‘bad’ seeing conditions and corresponds to a seeing disc size of 2.0 ± 0.1 arcseconds. Note how the image moves over a large area and has a mixture of low and high spatial frequencies. As a contrast, the right plot represents a seeing disc of only 0.9 ± 0.1 arcseconds. In this case the mirror position is more concentrated in one area.

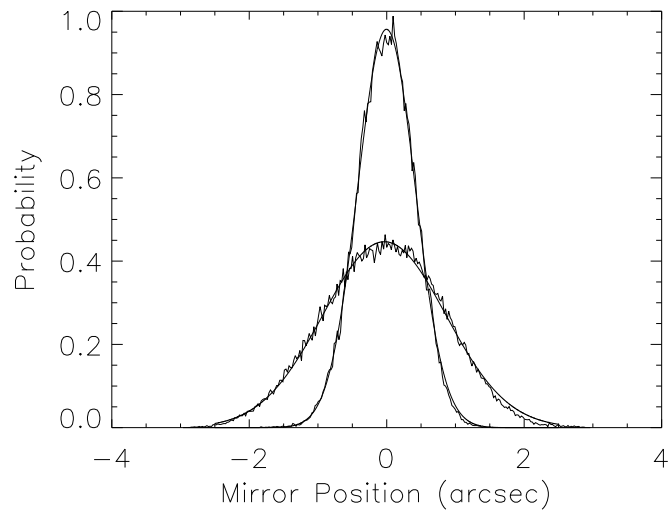


Figure 12: Two examples of seeing histograms, one for ‘bad’ and one for ‘good’ seeing conditions. A Gaussian curve fits these plots very well, allowing the measurement of the full width half maximum, the equivalent of a seeing disc.

4 Examples of Stellar Data

The control software, described in section 3.2, will log detector and mirror positions for later processing. A spare pair of digital to analogue converters also exists in the system hardware and these allow the real time monitoring of signals internal to the control computer. To illustrate the kind of data collected, two examples of mirror position data are given in Fig. 11, one representing bad seeing with a full width half maximum of 2.0 ± 0.1 arcseconds while the other represents average to good seeing of 0.9 ± 0.1 arcseconds.

The most common form of measurement of turbulent effects on telescopes is seeing disc size. Using one of the spare digital to analogue converters the position of one axis of one mirror can be monitored and measured using a dynamic signal analyser. This produces histograms of stellar image position, two examples of which are given in Fig. 12. The size of the seeing disc can be defined as the full width at half maximum of the resulting Gaussian fit. Seeing measurements of this kind have now been automated and are a regular part of the observational programme for SUSI. Some preliminary seeing statistics for the site have been published [2] and a fuller analysis will be presented when more data are available. This system also allows the measurement of tilt power spectra for the investigation of turbulence theory [2].

5 Conclusion

It is clear that the wavefront tilt correction servo described in this paper meets, and even exceeds, the design criteria set out in section 1. The servo has performed well in good and bad seeing, has been used to track stars of up to magnitude 6.5 and is predicted to reach magnitudes of up to 8.5. This performance compares favourably with other similar systems. The device was also shown to be capable of producing data for use in simple seeing studies and more complex investigations of turbulence theory.

Acknowledgments

The work presented in this paper was carried out during the development of the wavefront tilt correction system for SUSI. SUSI is funded jointly by the Australian Research Council and the University of Sydney with additional support from the Pollock Memorial Fund and the Science Foundation for Physics within the University of Sydney. Theo ten Brummelaar acknowledges the support of an Australian Postgraduate Research Award and thanks the CHARA group for assistance with the costs of producing this paper.

References

- [1] M. Born and E. Wolf *Principles of Optics* (Pergammon Press, Oxford, 1987)
- [2] T.A. ten Brummelaar, W.J. Tango, J.D. Davis and R.R Shobbrook, "A Preliminary Seeing Study for SUSI," Proceedings: I.A.U. Symposium 158, **Ed: Tango, W.J. and Robertson, J.G.**, Sydney (1993)

- [3] D.F. Buscher *Getting the most out of C.O.A.S.T.* (Cambridge University, Cambridge, 1988)
- [4] J. Davis and W.J. Tango, "The Sydney University 11.4m Prototype Stellar Interferometer," *Proc. A.S.A.*, **6**, 34-38 (1985)
- [5] J. Davis, W.J. Tango, A.J. Booth, R.A. Minard, T.A. ten Brummelaar and R.R T.A. Shobbrook, "An update on SUSI " in *Proceedings: High Resolution by Interferometry II*, Ed: Merkle, F. (1992)
- [6] J. Davis and W.J. Tango, "A New Very High Angular Resolution Stellar Interferometer," *Proc. A.S.A.*, **6**, 38-43 (1985)
- [7] J. Davis, "The Sydney University Stellar Interferometer," *Proceedings: I.A.U. Symposium 158*, **Ed: Tango, W.J. and Robertson, J.G.**, In Press (1993)
- [8] F.J. Dyson, "Photon Noise and Atmospheric Noise in Active Optical Systems," *J. Opt. Soc. Am.*, **65**, 551-558 (1975)
- [9] G.F. Franklin and J.D. Powell *Digital Control of Dynamic Systems* (Addison Wesley Pub. Comp., Reading MA., 1980)
- [10] N.S. Nightingale and D.F. Buscher, "Interferometric seeing measurements at La Palmer," *Mon. Not. R. astr. Soc.*, **251**, 155-166 (1991)
- [11] F. Roddier, "The Effects of Atmospheric Turbulence in Optical Astronomy," *Progress in Optics*, **XIX**, 281-376 (1981)
- [12] F. Roddier, J.E. Graves and E. Limburg, "Seeing Monitor Based on Wavefront Curvature Sensing " in *S.P.I.E. Proceedings: Advanced technology Optical Telescopes IV*, 1236 (1990), pp. 474-479.
- [13] R.Q. Twiss and W.J. Tango, "A New Michelson stellar interferometer," *Rev. Mex. Astron. Astrofis.*, **3**, 35-37 (1977)
- [14] G.A. Tyler and D.L. Fried, "Image-Position Error Associated with a Quadrant Detector," *J. Opt. Soc. Am.*, **72**, 804-808 (1982)
- [15] R.K. Tyson *Principles of Adaptive Optics* (Academic Press Inc., Boston, 1991)
- [16] J.F. Walkup and J.W. Goodman, "Limitations of Fringe-Parameter Estimation at Low Light Levels," *J. Opt. Soc. Am.*, **63**, 399-407 (1973)